Asian Journal of Research and Reviews in Physics

1(4): 1-11, 2018; Article no.AJR2P.45021

Shock Wave Interactions with Viscosity Observed after the Coronal Mass Ejection Activities Occurred on December 18, 1999 and April 4, 2001

Huseyin Cavus[1*] and Aysel Ibrahim Karafistan[2]

[1]Department of Physics, Faculty of Arts and Science, Canakkale Onsekiz Mart University, 17100, Canakkale, Turkey.
[2]Faculty of Maritime Management, University of Kyrenia, Sehit Yahya Bakir Sokak, Karakum-Girne, Post Box 74, Kyrenia TRNC, Cyprus.

Authors' contributions

This work was carried out in collaboration between both authors. Both authors read and approved the final manuscript.

Article Information

DOI: 10.9734/AJR2P/2018/v1i424632
Editor(s):
(1) Dr. Jelena Purenovic, Assistant Professor, Department of Physics and Materials, Faculty of Technical Sciences, Kragujevac University, Cacak, Serbia.
Reviewers:
(1) Yuan-Tsung Chen, National Yunlin University of Science and Technology, Taiwan.
(2) Snehadri B. Ota, University & Country Institute of Physics, India.
(3) Obiekea Kenneth Nnamdi, Ahmadu Bello University, Nigeria.
Complete Peer review History: http://www.sciencedomain.org/review-history/27371

Original Research Article

Received 09 September 2018
Accepted 19 November 2018
Published 23 November 2018

ABSTRACT

The release of magnetic field and plasma from the solar atmosphere (i.e. coronal mass ejections-CMEs and solar wind) resulting from solar magnetic activity can produce shock waves and geomagnetic storms. Shock waves are known to occur while the solar ejected particles alter from the supersonic to the subsonic regime. Especially, in the supersonic case for the flow of compressible gas interaction of shock waves with viscosity plays a key role for space weather broadcasts. Therefore, the major objective of this paper was to search the outcome of viscosity in the shocks subsequently detected after the CMEs occurred on December 18, 1999 and April 4, 2001 by using the previous modelling study of [1].

Keywords: Coronal mass ejection; viscosity; shock waves; reynolds number.

**Corresponding author: E-mail: h_cavus@comu.edu.tr, hu_cavus@hotmail.com;*

PACS Codes: 95.30.Lz 96.50.Fm 96.50.Ci 96.60.P-

1. INTRODUCTION

The solar atmosphere consisting of the photosphere, chromosphere, corona and the solar wind acceleration layers extend from the solar surface in the order of 10^0, 10^1, 10^1-10^2 and 10^3 Mm's respectively. The corona as the outermost part of the solar atmosphere is placed above the solar chromosphere layer. The temperature in the corona changes suddenly from a few thousand to a few million Kelvins [2] in the form of plumes, loops and streamers.

The corona is especially interesting with its complex magnetically 'closed' and 'open' structures. According to Priest [3] interaction between the magnetic field and the plasma characterises which kind of phenomena will occur. Closed magnetic loops located below the coronal streamers, may sometimes expand and coronal mass ejections (CME) in the form of an enormous plasma cloud can be ejected to the interplanetary space [4] and [5]. On the other hand, coronal holes result from the open plasma structures. In that case, a fast stream of plasma occurring in the fast solar wind spreads to the interplanetary space from the holes in the solar corona [6]. At such high coronal temperatures [3], the plasma will no more be constrained to the Sun gravitationally and will grow through the interplanetary medium at supersonic speeds as a solar wind. In his pioneering coronal expansion model, [7] predicted that high-speed solar wind can be observed near our Earth. Later, measurements of the solar wind parameters and improvements achieved in the theory led to the acceptance of the original idea. In the recent times, plumes appearing outside the coronal holes were suggested as possible reasons of the solar wind [8]. Interactions of these supersonic solar winds with the local interplanetary medium result in a shock wave. Amongst several ways to produce shocks in the solar wind are blast waves emitted from the Sun, CMEs and the interactions between the fast and slow streams [9]. Indeed, they may cause some changes in the physical conditions related to compression, heat, and changes in the magnetic field. Cavus and Kazkapan [10] studied the Kelvin-Helmholtz instability in the solar atmosphere and estimated the values of radial speed vary between 380 km/s and 780 km/s, for slow and fast solar winds respectively.

Another feature of the Sun is that it generates a continuous outflow of particles in the form of a high-speed solar wind which creates a shock wave in the sunward side after the collision with the planet's atmosphere. Shock waves result when particles in the solar wind are emitted at velocities 350-700 km/s [11], much higher than 100 km/s, the speed of sound in the interstellar medium [12] and [13]. Shocks arising from some of CMEs and solar winds were detected through the project of Solar and Heliospheric Observatory/The Large Angle and Spectrometric Coronagraph (SOHO/LASCO) and published by Stepanova and Kosovichev [14]. The expanding ejects travelling faster than ahead or behind the ambient gas will be a reason of a shock ahead and present a decreasing distribution of speed within ejects [15]. These shock properties were associated with the density compression features by Kilpua et al. [16].

Eselevich and Eselevich [17] showed that the CME's ahead frontal structure forms a disturbed region due to the CME's interaction with the undisturbed solar wind. The size of this region gradually increases as the CME travels away from the Sun and a narrow discontinuity region is observed to form at the disturbed zone of the front. Characteristics of this disturbed zone are similar to a piston shock which are collisional at the radial distances $r < 6R_{Sun}$ and collisionless for $r > 6R_{Sun}$ (where, R_{Sun} denotes the solar radius, and r is the distance from the centre of the Sun).

Some case studies of shock waves treated the complex entropy behaviour across the shock wave. For example, [18] studied entropy profile through the shock without viscosity and heat conduction effects. They showed that entropy increases in the shock front up to its maximum at the centre and then diminishes in the other half of the shock front. Even though this seems to violate the 2nd law of thermodynamics, it is still valid for the whole system, since entropy increases in the downstream region of the shock wave. Later, [19] studied entropy behaviour across the shock waves in a typical dusty gas precedent of the Navier-Stokes equations. He has found that the entropy distribution has its greatest value within the shock front and is increasing over the shock wave with respect to the upstream Mach number and the particle density. As a case study, [20] studied entropy in the shock wave that occurred after the CME of 12/12/2006 by the model described in [1].

The NASA- Advanced Composition Explorer (ACE) spacecraft routinely observe the events mentioned above. The ACE observatory, a spinning spacecraft (5 rpm), will orbit around the Sun- Earth L1 libration point (i.e. 240 times of the Earth radius). In order to get rid of the effects of the Earth's magnetic field, the ACE spacecraft has travelled almost a1.5 million km from the Earth. As another example [15] and [16] studied the shock waves that occurred after the CMEs of 18 February 1999 and 28 April 2001, which were accompanied by a flare and coronal waves. In the present paper various models of [1], [20-23] are applied to the shock wave that happened after these CMEs. Necessary values for the physical parameters are taken from the ACE mission and used as an upstream condition.

Initially, the model of [24] intended to study and predict the arrival of the shock waves on Earth. Unlike their study, the major aim of this article is to search the effects of viscous flows for the shock wave that happened after these two CMEs. In order to describe such shock processes, the Navier-Stokes equations are solved mathematically by means of the hydrodynamic model explained in [1]. In this modelling approach, viscous behaviour of a gas is considered as a function of the Reynolds number [1], [25] and [26]. In section 3, the downstream characteristics of the shock waves that occurred after the CMEs of February 18 1999 (hereafter CME18/02/1999) and April 28 2001 (hereafter CME28/04/2001) will be given. Results will be compared with other works in Section 4, and the conclusion will be driven after the discussions.

2. MODEL FORMULATION

2.1 Physical Parameters

Structure of the solar atmosphere is characterised with respect to the dominant roles played by the complex plasma and magnetic pressures, described by the plasma β parameter which is the ratio of the plasma pressure to the magnetic pressure. In other words, plasma pressure dominates over magnetic pressure, if β is greater than 1, and for the contrary case magnetic pressure dominates over that of the plasma. This ratio varies as a function of the magnetic field, reaches β>>1 values in the solar wind acceleration region, considered as infinity by Gary [27], and in the work of Matthaeus et al. [28] changes from 44 to infinity. In this context, importance of gas pressure in the dynamical modelling of the solar wind is well revised by Gonzales-Esparza et al. [29].

The CME interval is identified by the recombination of the enhanced density, temperature and velocity profiles. In the present work, upstream parametric values for different shocks that happened after the CME18/02/1990 and CME28/04/2001 are taken from the ACE spacecraft, listed in Table 1 [15] and [16].

They are employed in the model of [1] in order to examine effects of viscosity in these shocks.

In many cases, behaviour of the density data gives a guide to the occurrence and arrival of the shocks [24]. In Table 1, velocities are estimated as 390 km/s and 445 km/s for the cases of CME18/02/1999and CME28/04/2001, respectively. Since the local sound speed in the interplanetary medium is about 100 km/s [13], the shock wave should come into existence in this region, with temperatures around $1x10^5$ Kelvin and $5x10^4$ Kelvin respectively, at the start (Table 1).

2.2 Basic Formulae

The plasma β parameter defined as,

$$\beta = \frac{p_{gas}}{p_{mag}} \tag{1}$$

have values higher than one in the solar wind [27-30], since, the gas pressure of the plasma is dominant over the magnetic pressure, at such high coronal temperatures. This reduces the formulation of the wind problem to the hydrodynamic case explained in the pioneering work of [31] and later [32].

Thus, for a more generalised viscous shock in steady flow [1] obtained:

$$[(\frac{1}{2}-\frac{4}{3}\frac{1}{Re_1})(\gamma-1)M_1^2+1]\kappa^2-[(1-\frac{4}{3}\frac{1}{Re_1})\gamma M_1^2+1]\kappa+(\frac{\gamma+1}{2}-\frac{4}{3}\frac{1}{Re_2})M_1^2=0 \tag{2}$$

Table 1. Upstream values of physical parameters for two different shocks, after the CME18/02/1990 and CME28/04/2001 [15] and [16]

	n_1 (cm^{-3})	T_1 (Kelvins)	u_1 (km/s)
CME18/02/1999	3	1×10^5	390
CME28/04/2001	3.43	5×10^4	445

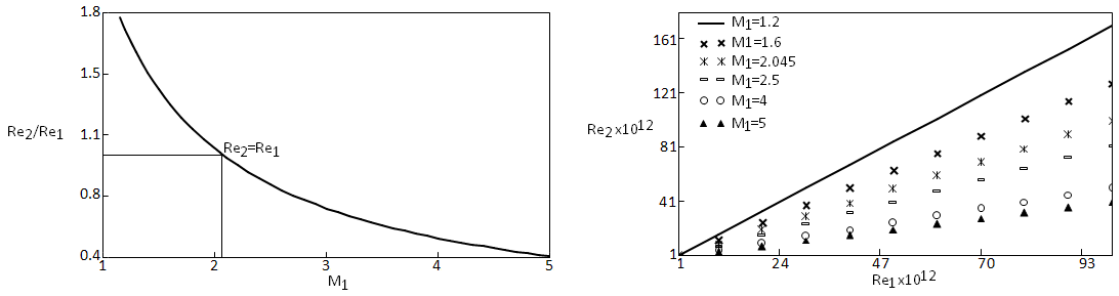

Fig. 1. Changes of the downstream Reynolds number (Re_2) as a function of the upstream Mach number M_1 (left) and the upstream Reynold's number Re_1 (right) [21]

In equation (2), Re_1 and Re_2 are the up and downstream Reynolds numbers (denoted by subscripts 1 and 2, respectively). The ratio of specific heats is given by γ, ratio of downstream to upstream densities (i.e. κ) and the upstream Mach number is represented by M_1. Effects of M_1, Re_1 and Re_2 parametric values on the distributions of the downstream physical parameters are considered here. According to Eselevich and Eselevich [33], for a collisionless shock γ ranges as $5/3 < \gamma < 3$. Then using the Rankine-Hugoniot jump formulas relations, [34] found the downstream physical parameter values. In which, they describe the relationship between the states on both sides of a shock wave in fluids. Similar to Cavus and Kurt [20], changes in entropy (S_2-S_1) can be evaluated in terms of the pressure ratios to the compression rate as follows:

$$S_2 - S_1 = c_v \ln\left[\frac{p_2}{p_1}\kappa^{-\gamma}\right] \quad (3)$$

2.3 Downstream Reynolds Numbers in the Solar Wind

Consequently, the Reynolds number with (Re>>1) values in the solar wind, plays a key role on the dynamics of this region. It is indicated to jump to 10^{12} and 10^{14} in the solar wind speeding up region by [8] and [35].

For simplification, the downstream Reynolds number, Re_2, is expressed as a function of γ, Re_1 and M_1 as [1] and [26]. The ratio Re_2/Re_1 given as a function of M_1 in the left side of Fig. 1, is decreasing as the upstream Mach number increases and equals to unity (i.e. Re_1=Re_2) for $M_1\approx2$. The latter can be considered as a transition region from weak to strong shocks, since for weak shocks M_1<2, and for strong shocks M_1>2 [1] and [36].

In the right panel of Fig. 1, variation of Re_2 according to Re_1 for various M_1 values, is given for the case of a monatomic gas of γ=5/3 [21]. In the same manner described by Borovsky and Funsten [8] and Veselovsky [35] Reynolds number Re_2 can be deduced and seen to increase with increasing Re_1 ending with greater values for smaller M_1.

3. MODELLING RESULTS FOR THE SHOCKS HAPPENED AFTER THE CME18/02/1999 AND CME28/04/2001

Some particular solutions of the equations (2-3) and the Rankine-Hugoniot jump formulas [34] were adapted to a symbolic and numeric computing environment Maple 9.5, in order to derive the downstream parameter values for the shock waves driven by the CME18/02/1999 and CME28/04/2001. The downstream physical parameters thus found are represented either in Table 2 or in Figures (Figs. 2-8). The upstream Reynolds number used in our solar wind calculations is taken as 10^{13} [8,37] and [38].

Table 2. Variations of the basic physical parameters as a function of M_1

M_1	Re_2/Re_1	n_2/n_1	u_2/u_1	T_2/T_1	S_2-S_1	M_2/M_1
1.200	1.704	1.297	0.771	1.195	0.055	0.705
1.600	1.278	1.842	0.543	1.602	0.798	0.429
2.045	1.000	3.329	0.437	2.137	2.441	0.294
2.500	0.818	2.703	0.370	2.798	4.566	0.221
4.000	0.511	3.368	0.297	5.863	11.961	0.123
5.000	0.409	3.571	0.280	8.680	16.368	0.095

Basic physical model is parameterised in Table 2 as a function of M_1. As before these are expressed as a function of ratios for the Reynolds numbers (Re_2/Re_1), κ (i.e. density ratios, n_2/n_1), velocity ratio (u_2/u_1), ratios of temperature (T_2/T_1), and the Mach numbers ratio (M_2/M_1) together with the entropy difference (S_2-S_1), all obtained from the solutions of equation (2) and the application of the jump conditions. For the case of M_1=2.045, equating the Reynolds numbers ratio to unity, the critical Mach number for the turning point is found (see Fig. 1). As indicated by Cavus [1], this point is not only important for the Reynolds numbers ratio but also for the strength of the shock waves. Decreasing trends of Re_2/Re_1, u_2/u_1 and M_2/M_1 with increasing M_1, is seen to slow down after the critical Mach number M_1=2.045 is reached. On the other hand, density and temperature ratios together with the entropy differences tend to increase with increasing M_1 which slows down for n_2/n_1, speeds up for T_2/T_1 and S_2-S_1 after the point M_1=2.045 is reached.

Using the corresponding upstream density values given in Table 1 downstream density dependencies are obtained as a function of M_1 and Re_2/Re_1 and drawn for the two case studies in the left and right panels of Fig. 2, respectively. Again as expected n_2 is increasing with higher upstream Mach number, but density is inversely proportional to the increasing Reynolds number ratios Re_2/Re_1, [1]. For weak shocks (i.e. M_1<2) this variation seems to be linear and nonlinear for strong shocks (i.e. M_1>2). In the extreme case of M_1=5, n_2 reaches the values of 10 $cm^{-3}$for the CME18/02/1999, 12 cm^{-3} for the CME28/04/2001 (Fig. 2).

Fig. 3 represents downstream temperature changes as a function of M_1 and Re_2/Re_1. These changes are small for the weak shock region (i.e. M_1<2) compared to the variations in the strong shocks (M_1>2). The upstream temperature values given in Table 1(1×10^5 and 5×10^4 Kelvin) are used to calculate the downstream temperature T_2, which tends to increase for the upstream Mach number, M_1=5, and exhibits small variations for M_1<2 increasing again for M_1>2 (see also Table 2) Finally, for the higher values of M_1 related to CME18/02/1999 and CME28/04/2001, T_2 reaches 8.68×10^6 Kelvin and 4.34×10^5 Kelvin, respectively.

In Fig. 4 variation of the downstream velocity u_2 is depicted as a function of M_1 (left panel) and Re_2/Re_1 (right panel). The upstream values directly taken from Table 1, are both observed to have decreasing tendencies. Unlike T_2, changes in u_2 are large for the weak shock case (i.e. M_1<2), compared to the changes in the strong shocks (M_1>2).

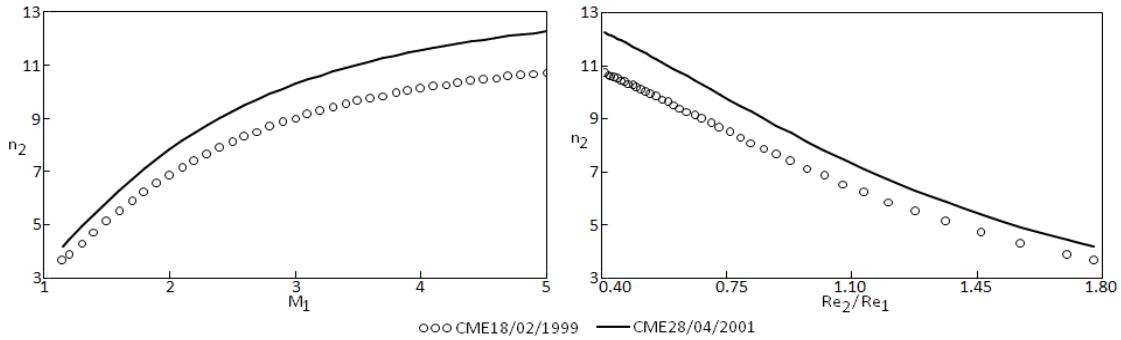

Fig. 2. Changes in the downstream density (in cm^{-3}) as a function of M_1 (left) and Re_2/Re_1 (right) for both the CME18/02/1999 and CME28/04/2001

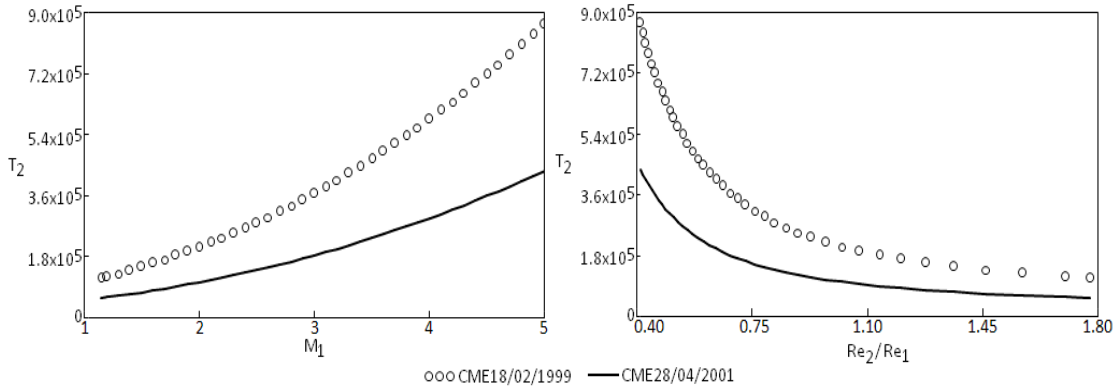

Fig. 3. Downstream temperature changes T_2 (in Kelvin) drawn as a function of M_1 (left) and Re_2/Re_1 (right) values of CME18/02/1999 and CME28/04/2001

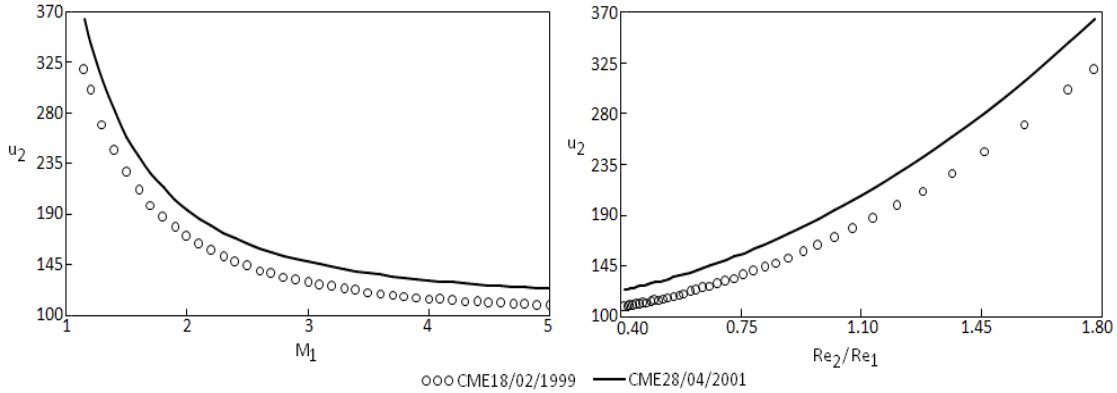

Fig. 4. Variation of u_2 with respect to M_1 (left) and Re_2/Re_1 (right) values

Fig. 5 shows changes in some parameters with respect to the entropy differences, where the cross symbols representing temperature ratios of the downstream to the upstream values (T_2/T_1), are observed to increase with the entropy difference. The empty squares depict the compression ratio (n_2/n_1) exhibit a similar behaviour with the sound speed, increases with S_2-S_1, whereas the Re_2/Re_1 ratio, (empty triangles) have a decreasing tendency. On the other hand, the downstream to upstream velocity ratios (u_2/u_1) represented by plus signs is also decreasing with increasing entropy differences. All of these ratios are unity for S_2-S_1=0 (i.e. the isentropic case). Finally, all of these ratios become unity for the isentropic case (S_2-S_1=0), which means that no shock occurs for the case with no compression (κ=1).

Downstream density variation is presented in Fig. 6 as a function of the entropy difference where S_2-S_1<2.44 corresponds to the weak shock (M_1<2) region in Table 2. As expected the downstream density variations (n_2) increase with entropy differences S_2-S_1 but these variations are small for further increase of the S_2-S_1. On the other hand, from the S_2-S_1 dependence of T_2 shown in Fig. 7 tends to increase with increasing entropy differences. The T_2 changes are small for the weak shock region (S_2-S_1<2.44) compared to the changes in the strong shocks (S_2-S_1>2.44).

From Fig. 8 we observe a decreasing tendency of the downstream velocity (u_2) for greater entropy differences (S_2-S_1) as expected, whereas u_2 variations are small for larger S_2-S_1 differences. Again the very weak shocks are closely isentropic when S_2 is nearly equal to its upstream value given in Table 2 and this variation is high when M_1>>2 happens for strong shocks.

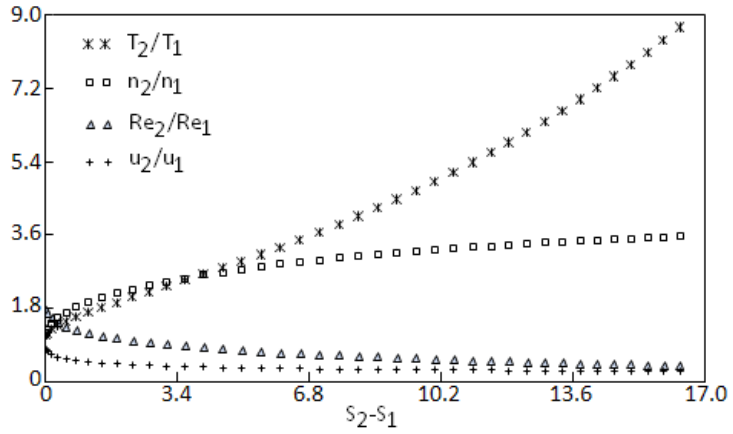

Fig. 5. Variations of some parameters with respect to the entropy difference S_2-S_1

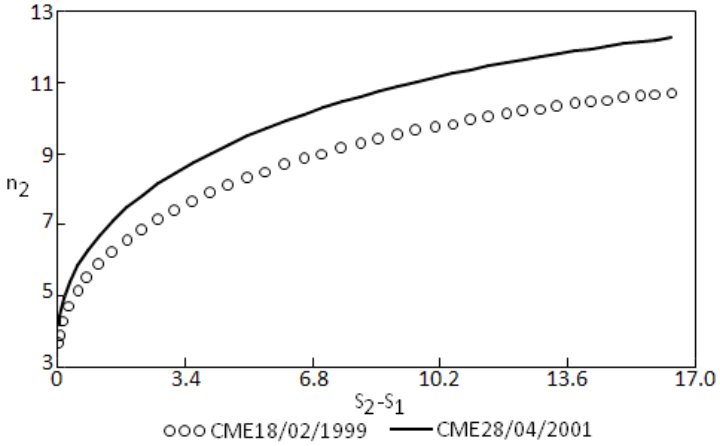

Fig. 6. Downstream density variation with respect to entropy difference S_2-S_1 for CME18/02/1999 and CME28/04/2001

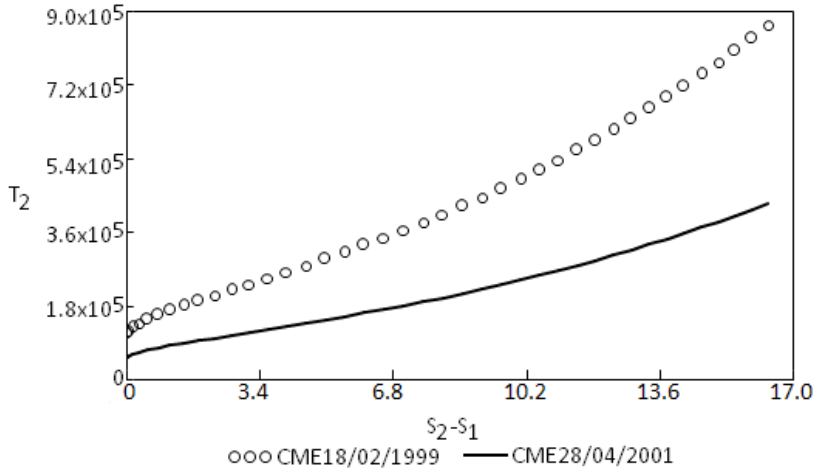

Fig. 7. Variations o T_2 as a function of S_2-S_1 for the CME18/02/1999 and CME28/04/2001

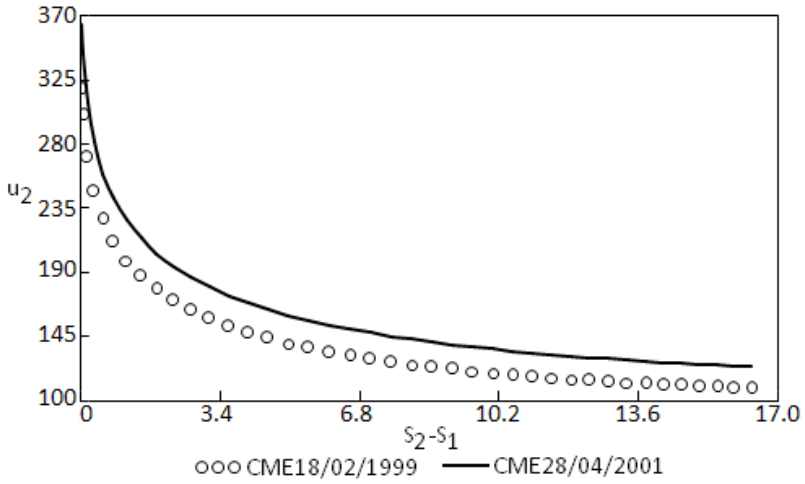

Fig. 8. Variations of u_2 as a function of S_2-S_1 for the CME18/02/1999 and CME28/04/2001

4. DISCUSSION AND CONCLUSION

Investigation of CME driven shocks waves from the Sun to the interplanetary space is important for space weather forecasting since sufficient energy is released very rapidly capable to produce a ‘‘fast’’ CME which can drive an interplanetary shock [15]. On the other hand, understanding behaviour and change of the physical parameters, describing these phenomena still stays a very sophisticated task relevant to the present observational facts.

As far as we know when a CME explodes in the corona, besides the interactions with the ambient interplanetary gas, more complex magnetic and thermal energy processes occur. Even though the magnetic pressure dictates near the Sun, gas pressure becomes more dominant beyond the Sun. Then, the hydrodynamical modelling approach is adequate for the study and evaluation of the CME driven shock in the solar wind [27-29] and [39].

With this context in mind, two different shock waves that occurred after the CME18/02/1999 and CME28/04/2001 are studied here. Evolution of the shock propagation in the surrounding space is analysed by means of a 1-D hydrodynamical model, parameterised with respect to the Reynolds number effects. From our results we can draw the following conclusions presented as items:

- Comparing our result, with that of [15] we deduced that the downstream plasma density 10.3 cm^{-3} fits well to $M_1 \approx 4.4$ in the present model presented by Figure 2. The downstream density value approximated as 12.2 $cm^{-3}$by [16] corresponds to $M_1 \approx 4.9$ in our model. All these fit well the shock properties produced after the CME18/02/1999 and CME28/04/2001 events which should have both occurred as very strong shocks ($M_1>4$). The strengths of these shocks show that our theoretical calculations are very close to the practical ACE satellite measurements.
- For the above shocks the Reynolds number ratios, Re_2/Re_1, are evaluated as 0.46 and 0.41 respectively with the upstream Mach number given in Fig. 1. From these two results we conclude that $Re_2<Re_1$, which means the upstream is more turbulent than the downstream [36] for both CMEs.
- As Re_2/Re_1 increases the ratio of kinematic viscosities (i.e. ν_1/ν_2) increases. In other words, upstream of the shock becomes more viscous ($\nu_1>\nu_2$). Figs. 2 and 3 show that, T_2 and n_2 decrease with increasing values of ν_1. In Fig. 4, we observe a increasing tendency of the downstream velocity (u_2) for greater values of ν_1/ν_2 as expected.
- The compression rates (κ) of these shock waves are greater than 3.5 for the two cases.

- The aftershock velocities are estimated as 112 km/s and 125 km/s for the CME18/02/1999 and CME28/04/2001 respectively (see Fig. 5).
- When we employ the upstream Mach numbers 4.4 and 4.9, and the upstream velocities given in Table 1, the sound speeds in the interplanetary medium are found as 89 km/s and 91 km/s for the two cases which are comparable to the works of [12] and [13], who estimated this value within the range 90-100 km/s.
- The entropy difference, S_2-S_1, is found to increase with increasing upstream Mach number M_1. Similar to [20] and [40] very weak shocks (i.e. M_1<1.2) turn into become nearly isentropic for the increasing values Reynolds number ratios (Re_2/Re_1).
- Entropy difference S_2-S_1 has a tendency to increase with increasing compression rate (κ), which means that the downstream density itself is increasing with the entropy difference.
- Downstream temperature also shows an increasing trend with greater entropy differences.
- On the other hand, unlike the κ and temperature ratio variations, the entropy differences S_2-S_1 decrease with increasing fluid velocity ratios.

ACKNOWLEDGEMENT

This paper was supported by TUBITAK 117F336 project.

COMPETING INTERESTS

Authors have declared that no competing interests exist.

REFERENCES

1. Cavus H. On the effects of viscosity on the shock waves for a hydrodynamical case — Part I: Basic Mechanism Advances in Astronomy. 2013;2013.
   DOI: 10.1155/2013/58296).
2. Parker EN. Heating solar coronal holes The Astrophysical Journal. 1991;372:719-727.
3. Priest ER. Solar Magnetohydrodynamics, D. Reidel Publishing Company, Dordrecht, Holland; 2000.
4. Antiochos SK, De Vore CR, Klimchuk JA. A model for solar coronal mass ejections. The Astrophysical Journal. 1999;510:485-493.
5. Shugay YS, Slemzin VA, Rod'kin DG. Features of solar wind streams on June 21–28, 2015 as a result of interactions between coronal mass ejections and recurrent streams from coronal holes Cosmic Research. 2017;55:389-395.
6. Stix M. The Sun, Springer Verlag; 1991.
7. Parker EN. Dynamics of the interplanetary gas and magnetic fields. The Astrophysical Journal. 1958;128:664-676.
8. Borovsky JE, Funsten HO. Role of solar wind turbulence in the coupling of the solar wind to the Earth's magnetosphere Journal of Geophysical Research. 2003; 108(A6):13-1 - 13-25.
9. Sturrock PA, Spreiter JR. Shock waves in the solar wind and geomagnetic storms Journal of Geophysical Research. 1965; 70:5345-5351.
10. Cavus H, Kazkapan D. Magnetic Kelvin-helmholtz instability in the solar atmosphere. New Astronomy. 2013;25:89-94.
11. Rouillard AP, Odstrcil D, Sheeley NR, Tylka A, Vourlidas A, Mason G, Wu CC, Savani NP, Wood BE, Ng CK, Stenborg G, Szabo A, Cyr OCSt. Interpreting the properties of solar energetic particle events by using combined imaging and modeling of interplanetary shocks. The Astrophysical Journal. 2011;735(7):1-11.
12. Suzuki T. Coronal heating and acceleration of the high/low-speed solar wind by fast/slow MHD shock trains. Monthly Notices of Royal Astronomical Society. 2011;349:1227-1239.
13. Nakariakov VM, Ofman L, Arber TD. Nonlinear dissipative spherical Alfvén waves in solar coronal holes. Astronomy and Astrophysics. 2000;353:741-748.
14. Stepanova TV, Kosovichev AG. Observation of shock waves associated with coronal mass ejections from SOHO/LASCO, Advances in Space Research. 2000;25(9):1855-1858.
15. Riley P, Linker JA, Mikic Z, Odstrcil D. Modeling interplanetary coronal mass

ejections. Advances in Space Research. 2006;38:535-546.

16. Kilpua EKJ, Isavnin A, Vourlidas A, Koskinen HEJ, Rodriguez L. On the relationship between interplanetary coronal mass ejections and magnetic clouds, Annales Geophysicae. 2013;31:1251-1265.
17. Eselevich V, Eselevich M. Disturbed zone and piston shock ahead of coronal mass ejection. The Astrophysical Journal. 2012; 761(68):1-10.
18. Morduchow M, Libby PA. On a complete solution of the one-dimensional shock wave structure. J. Aeron. Sci. 1949;16: 674-684.
19. Hamad H. Behavior of entropy across shock waves in dusty gases, Zeitschrift für angewandte Mathematik und Physik. 1998;49:827-837.
20. Cavus H, Kurt A. Effects of viscosity on the behavior of entropy change in the shock wave that occurred after the December 13, 2006 coronal mass ejection. Astrophysical Bulletin. 2015;70:220-225.
21. Cavus H. On the viscosity effects in the shock wave observed in the solar wind after the December 13, 2006 coronal mass ejection. Astrophysical Bulletin. 2015;70: 117-122.
22. Cavus H. Treatment of viscosity in the shock waves observed after two consecutive coronal mass ejection activities CME08/03/2012 and CME15/03/2012, Earth, Moon and Planets. 2016;118:91-101.
23. Cavus H, Zeybek G. Effect of viscosity on shock waves observed after two different coronal mass ejection activities CME20/11/2003 and CME11/04/2010, Astrophysics. 2017;60(1):100-110
24. Vandegriff J, Wagstaff K, Ho G, Plauger J. Forecasting space weather: Predicting interplanetary shocks using neural networks. Advances in Space Research. 2003;36(12):2323-2327.
25. Reynolds O. An experimental ınvestigation of the circumstances which determine whether the motion of water shall he direct or sinuous, and of the law of resistance in parallel channels. Philosophical Transactions of the Royal Society. 1883; 174:935-982.
26. Bruhn FC, Pauly K, Kaznov V. Proceedings of The 8th International Symposium on Artificial Intelligence, Robotics and Automation in Space (iSAIRAS), Munich-Germany; 2005.
27. Gary GA. Plasma beta above a solar active region: Rethinking the paradigm, 2003:1Solar Physics. 2003;71-86.
28. Matthaeus WH, Ghosh S, Oughton S, Roberts DA. Anisotropic three-dimensional MHD turbulence. Journal of Geophysical Research. 1996;101(A4): 7619-7629.
29. Gonzales-Esparza JA, Corona-Romero P, Aguilar-Rodriguez E. Proceedings of XXIX International Conference on Phenomena in Ionized Gases, Cancun-Mexico; 2009.
30. Tsiklauri D, Nakariakov VM, Arber TD. A strongly nonlinear Alfvénic pulse in a transversely inhomogeneous medium. Astronomy and Astrophysics. 2002;395: 285-292.
31. Parker EN. The stellar-wind regions. The Astrophysical Journal. 1961;134:20.-27.
32. Holzer TE, Axford WI. The theory of stellar winds and related flows. Annual Reviews of Astronomy and Astrophysics. 1970;8: 31-60.
33. Eselevich MV, Eselevich VG. Relations estimated at shock discontinuities excited by coronal mass ejections, Astronomy Reports. 2011;155:359-373.
34. Zel'dovich YB, Raizer YP. Physics of shock waves and high-temperature hydrodynamic phenomena. Dover Publications Inc., New York; 2002.
35. Veselovsky I. Turbulence and waves in the solar wind formation region and the heliosphere. Astrophysics and Space Science. 2001;277:219-224.
36. Warsi ZUA. Fluid dynamics: Theoretical and computational approaches. Boca Raton Fla., CRC Press; 1999.
37. Heinemann M. Effects of solar wind inhomogeneities on transit times of interplanetary shock waves. Journal of Atmospheric and Solar-Terrestrial Physics. 2002;64:315–325.
38. Oliveira DM, Raeder J, Tsurutani BT, Gjerloev JW. Effects of ınterplanetary shock ınclinations on nightside auroral power ıntensity. Brazilian Journal of Physics. 2016;46(1):97-104.

39. Zong QG, Zhou XZ, Wang YF, Li X, Song P, Baker DN, Fritz TA, Daly PW, Dunlop M, Pedersen A. Energetic electron response to ULF waves induced by interplanetary shocks in the outer radiation belt. J. Geophys. Res. 2009;114(A10204): 1-11.

40. Liu Y, Luhmann JG, Müller-Mellin R, Schroeder PC, Wang L, Lin RP, Bale SD, Li Y, Acuna MH, Sauvaud JA. A comprehensive view of the 2006 December 13 CME: From the Sun to Interplanetary Space. The Astrophysical Journal. 2008;689:563-571.

Peer-review history:
The peer review history for this paper can be accessed here:
http://www.sciencedomain.org/review-history/27371